A Dual-Layer Dispatch Framework for Concentrated Solar Power Systems Considering Molten Salt Thermodynamics

Yan Xu
Department of Engineering Mechanics
Tsinghua University
Beijing, China
1002171834@qq.com

Zhengfeng Shuai
China Three Gorges Renewables(Group)Co.,Ltd
Beijing, China
shuai_zhengfeng@ctg.com.cn

Feng Tian
China Three Gorges Renewables(Group)Co.,Ltd
Beijing, China
tian_feng1@ctg.com.cn

Yongnian Yang
China Three Gorges Renewables(Group)Co.,Ltd
Beijing, China
yang_yongnian@ctg.com.cn

Lin Shi
China Three Gorges Renewables(Group)Co.,Ltd
Beijing, China
shi_lin1@ctg.com.cn

Hongshan Liu
China Three Gorges Renewables(Group)Co.,Ltd
Beijing, China
liu_hongshan@ctg.com.cn

Huan Ma*
Department of Engineering Mechanics
Tsinghua University
Beijing, China
mahuaneea@outlook.com
*Corresponding author

Qun Chen
Department of Engineering Mechanics
Tsinghua University
Beijing, China
chenqun@tsinghua.edu.cn

2025 7th Asia Energy and Electrical Engineering Symposium (AEEES) | 979-8-3315-1754-0/25/$31.00 ©2025 IEEE | DOI: 10.1109/AEEES64634.2025.11020088

***Abstract*—Concentrated Solar Power (CSP) plants with integrated thermal energy storage systems are critical for renewable energy dispatchability, yet their operational efficiency is challenged by frequent fluctuations in solar irradiance and power generation load, which propagate dynamic temperature variations in molten salt across hot and cold storage tanks. Existing optimization approaches oversimplify these interactions, neglecting the coupled effects of solar irradiance variability, molten salt discharge flow rates, and molten salt temperature changes on thermoelectric conversion efficiency. To address this, we propose a dual-layer optimization-simulation framework that decouples CSP operations into two coordinated subproblems: (1) a thermal dynamics simulation layer modeling real-time molten salt temperature evolution via irradiance-adaptive flow control, and (2) a power generation optimization layer scheduling electricity output based on the molten salt thermal state. Through iterative coordination, the method prioritizes power generation during high thermal potential periods (hot tank outlet temperature exceeding time-weighted averages), with experimental validation on a 110MW CSP plant demonstrating 985.43 MWh daily generation at 8188.32 kJ/kWh specific heat consumption, achieving a 2.2% efficiency improvement over simplified models by neglecting flow control cycles and thermal dynamics of molten salt.**

Keywords—Concentrated Solar Power (CSP) plant; Optimization Scheduling; Molten Salt Dynamics; Dual-layer Iterative optimization; Temperature and Flow Rate Constraints

I. INTRODUCTION

Amid growing climate and environmental challenges, fossil fuel use has driven significant greenhouse gas emissions, worsening extreme weather and ecosystem degradation[1]. To achieve carbon peak and neutrality goals, renewable energy development has become central to the global energy transition. However, intermittent sources like solar and wind face challenges due to their randomness and volatility[2]. Concentrated Solar Power (CSP), with integrated solar collection, storage, and generation, offers unique advantages in stabilizing power systems [3]. Recently, CSP has gained attention as a key pathway for low-carbon energy transformation.

In peak shaving scenarios, CSP units often operate under varying conditions, significantly affecting efficiency. To balance flexibility and efficiency, a comprehensive model reflecting CSP's complex constraints and efficiency variations under dynamic conditions is needed. Recent studies have proposed various CSP operation models. Reference [4] introduced a modified model for molten salt-driven Rankine cycles, validated via SAM software, to predict performance under different conditions. Reference [5] built a global CSP database, optimizing plant design in arid climates using SolarPILOT and SAM, including heliostat layout, collector size, and thermal storage configuration.

The optimization scheduling of CSP plants is key to maximizing their economic and technical benefits. As electricity markets shift from fixed-price subsidies to market-driven pricing, CSP scheduling strategies must become more flexible and efficient. Reference [6] proposed a nonlinear optimization model, showing that optimized configurations and flexible operations enhance economic performance despite market fluctuations. Reference [7] evaluated CSP's techno-economic feasibility in spot markets, finding thermal storage tanks optimal for financial performance. CSP's coordination with other energy systems, such as CHP units, balances grid demand and renewable variability [8]. Reference [9] introduced a joint CSP-CHP model, reducing costs and improving flexibility through multi-timescale stochastic optimization. Reference [10] explored CSP's heating potential, using IGDT to address uncertainty. Reference [11] proposed a two-layer optimization

This work was supported by Scientific Research Project
Supported by China Three Gorges Renewables (Group) Co., Ltd (62035004).

Authorized licensed use limited to: University of Pittsburgh. Downloaded on July 07,2026 at 17:40:39 UTC from IEEE Xplore. Restrictions apply.

model combining thermal storage and SOPs, enhancing grid stability and economics. CSP-based hybrid systems stabilize grids and reduce fossil fuel reliance, especially with fluctuating wind and PV [12]. Reference [13] developed a multi-stage ARO model for CSP-wind joint scheduling, reducing costs and curtailment rates. Reference [14] optimized wind-PV-CSP systems using IPSO, showing CSP improves economics and stability. Reference [15] proposed a clean energy optimization model with CSP regulation, increasing wind and PV utilization.

Existing CSP optimization methods often use simplified models to avoid complex non-linear problems. These models focus on energy balance but neglect critical factors like temperature- and flow-dependent efficiencies, dynamic molten salt temperature profiles, and transient flow variations. Process constraints, such as DNI limits and pump flow rates, significantly affect molten salt temperature at the collector outlet. The system compares this temperature to a threshold to decide whether the molten salt enters the hot or cold tank for mixing. These parameters directly impact thermal storage performance and steam power generation efficiency. Current strategies trade physical accuracy for computational speed, which becomes problematic in real-world scenarios like peak shaving, leading to deviations between performance and design assumptions, compromising accuracy and safety.

This research proposes a novel CSP optimization framework integrating process constraints and efficiency variations into a unified hierarchy. The problem is decomposed into two subproblems: a multi-objective optimization model for thermal release and power scheduling, and a high-fidelity simulation platform capturing salt flow, temperature, and efficiency dynamics. These subsystems are solved iteratively through a coordinated loop, enabling revenue-maximizing strategies under dynamic grid demands. By decoupling non-linear models and using surrogate-based optimization, the approach achieves real-time optimization without full integration of complex physical models.

II. Simulation Model CSP Plant

A typical tower-type CSP system consists of three core components: a concentrating solar collector system, a thermal storage system, and a power generation system. The collector system captures and converts solar radiation into thermal energy. The thermal storage system, acting as an "energy intermediary," stores heat in molten salt during surplus solar irradiance and releases it during demand to generate steam for power. The power generation system includes steam turbines and generators to convert thermal energy into electricity. This research will develop mathematical models for each subsystem.

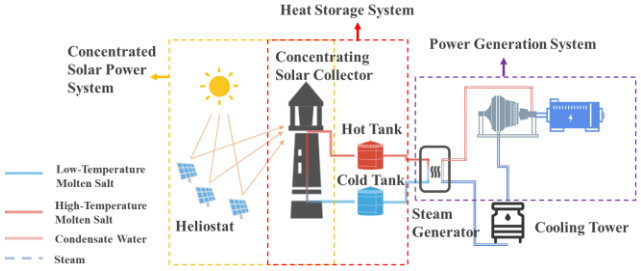

Fig. 1. Schematic diagram of the CSP system

A. Concentrating Solar Collector

The core process involves the heliostat field reflecting solar radiation onto the collector, which heats the working fluid from a low to a high temperature. The heated fluid is stored in the thermal energy system, enabling efficient solar conversion and controllable storage.

$$Q_{\mathrm{inc},t} = I_{\mathrm{DNI},t} S_{\mathrm{HF}} \eta_{\mathrm{ref}} \eta_{\mathrm{att}} \tag{1}$$

$$Q_{\mathrm{recv,out},t} = \alpha Q_{\mathrm{inc},t} - Q_{\mathrm{loss},t} \tag{2}$$

$$Q_{\mathrm{loss},t} = h_{\mathrm{R}} A_{\mathrm{R}} \left(T_{\mathrm{W}} - T_0\right) + \sigma \varepsilon_{\mathrm{R}} A_{\mathrm{R}} T_{\mathrm{W}}^4 \tag{3}$$

$$m_{\mathrm{recv,in},t} = \frac{Q_{\mathrm{recv,out},t}}{C \Delta T} \tag{4}$$

In the equation, $I_{\mathrm{DNI},t}$ is direct solar radiation, measured in W/m². S_{HF} is the heliostat field's total illuminated area in m². η_{ref} is heliostat reflectance, and η_{att} is atmospheric transmittance. $Q_{\mathrm{recv,out},t}$ is the net thermal output of the solar collector in J. $Q_{\mathrm{inc},t}$ is the thermal reaching the collector's surface in J. α is the collector's efficiency. $Q_{\mathrm{loss},t}$ is the total thermal loss, including radiative and convective losses, in J. h_{R} is the convective heat transfer coefficient in W/(m²·K). A_{R} is the collector's illuminated area in m². T_{W} is the average wall temperature in K, and T_0 is the ambient temperature in K. σ is the Stefan-Boltzmann constant in W/(m²·K⁴). ε_{R} is the collector's emissivity. $m_{\mathrm{recv,in},t}$ is the molten salt flow rate from the cold tank in kg/s, and ΔT is the temperature change of the molten salt after heating in °C. Equation (1) quantifies the radiative energy absorbed by the solar collector, considering atmospheric attenuation and heliostat mirror efficiency. Equation (2) calculates the net output power, derived from the concentrated energy $Q_{\mathrm{inc},t}$ minus thermal losses, representing the energy transferred to the thermal medium. Equation (3) computes convective and radiative thermal losses. The solar collector heats the molten salt, with its flow rate determined by the required temperature rise to achieve the desired outlet temperature, as shown in Equation(4).

B. Hot Tank

The high-temperature thermal storage tank operates in two phases: first, molten salt is pumped into the tank for storage when the solar collector reaches a thermal threshold; second, during peak demand, the molten salt is extracted and sent to the heat exchanger for power generation.

$$M_{\mathrm{hot,left},t} = M_{\mathrm{hot},t\text{-}1} - m_{\mathrm{hot,out},t} \Delta t \tag{5}$$

$$T_{\mathrm{hot},t} = \frac{m_{\mathrm{recv,in},t} T_{\mathrm{recv,out},t} \Delta t + M_{\mathrm{hot,left},t} T_{\mathrm{hot},t-1}}{m_{\mathrm{recv,in},t} T_{\mathrm{recv,out},t} + M_{\mathrm{hot,left},t}} \tag{6}$$

$$M_{\mathrm{hot},t} = M_{\mathrm{hot,left},t} + m_{\mathrm{recv,in},t} \Delta t \tag{7}$$

$$M_{\mathrm{hot},t+1} = M_{\mathrm{hot},t} + \left(m_{\mathrm{sto},t} - m_{\mathrm{rel},t}\right) \Delta t \tag{8}$$

$$M_{\mathrm{hot,min}} \le M_{\mathrm{hot},t} \le M_{\mathrm{hot,max}} \tag{9}$$

$$m_{\mathrm{rel,min}} v \le m_{\mathrm{rel},t} \le m_{\mathrm{rel,max}} v \tag{10}$$

Authorized licensed use limited to: University of Pittsburgh. Downloaded on July 07,2026 at 17:40:39 UTC from IEEE Xplore. Restrictions apply.

In the equation, $M_{\text{hot,left},t}$ represents the mass of molten salt remaining in the thermal tank at time t after entering the steam generator, kg. $M_{\text{hot},t}$ denotes the mass of molten salt in the thermal tank at time t, kg . $m_{\text{hot,out},t}$ indicates the flow rate of molten salt leaving the thermal tank and entering the steam evaporator at time t, kg/s. t represents time, s. In the equation, $T_{\text{hot},t}$ represents the temperature of the molten salt in the thermal storage tank at time t , K. $T_{\text{recv,out},t}$ represents the temperature of the molten salt flowing into the thermal storage tank after being heated by the solar collector at time t, K. $M_{\text{hot,min}}$ represents the lower limit of the molten salt mass in the hot tank, kg. $M_{\text{hot,max}}$ represents the upper limit of the molten salt mass in the hot tank, kg. When there is a load demand, high-temperature molten salt is pumped from the hot tank to the steam exchanger for thermal exchange. The change in molten salt mass in the hot tank is represented by(5). After absorbing heat in the solar collector, the molten salt reaches the desired outlet temperature and is pumped into the hot tank for storage, mixing with existing salt. The temperature mixing and mass change in the hot tank are described by (6) and (7), respectively. Equation (8) represents mass conservation in the hot tank, while (9) and (10) define constraints on molten salt mass and thermal release flow rate, ensuring they stay within specified bounds.

C. Cold Tank

The low-temperature thermal storage system operates in three phases: during solar irradiation, cold salt circulates through the solar collector to absorb heat. Once reaching the optimal temperature, it is stored in the hot tank. If the temperature threshold is unmet, underheated salt is recirculated to the cold tank for mixing. Meanwhile, molten salt from the heat exchanger returns to the cold tank for continuous storage.

$$M_{\text{cold,left},t} = M_{\text{cold},t\text{-}1} - m_{\text{recv,in},t}\Delta t \tag{11}$$

$$T_{\text{cold},t} = \frac{T_{\text{recv,out},t} m_{\text{recv,in},t}\Delta t + M_{\text{cold,left},t} T_{\text{cold},t\text{-}1} + T_{\text{cold,in},t} m_{\text{hot,out},t}\Delta t}{m_{\text{recv,in},t}\Delta t + M_{\text{cold,left},t} + m_{\text{hot,out},t}\Delta t} \tag{12}$$

$$M_{\text{cold},t} = m_{\text{recv,in},t}\Delta t + M_{\text{cold,left},t} + m_{\text{hot,out},t}\Delta t \tag{13}$$

$$M_{\text{cold},t+1} = M_{\text{cold},t} + \left(m_{\text{rel},t} - m_{\text{sto},t}\right)\Delta t \tag{14}$$

$$M_{\text{cold,min}} \le M_{\text{cold},t} \le M_{\text{cold,max}} \tag{15}$$

In the equation, $M_{\text{cold,left},t}$ is the remaining molten salt mass in the cold tank after entering the collector, in kg. $M_{\text{cold},t}$ is the molten salt mass in the cold tank at time t, in kg. $T_{\text{cold},t}$ is the molten salt temperature in the cold tank at time t, in K. $T_{\text{cold,in},t}$ is the temperature of molten salt returning to the cold tank after thermal release, in K. $M_{\text{cold,min}}$ and $M_{\text{cold,max}}$ are the lower and upper limits of molten salt mass in the cold tank, in kg. Equation (11) describes the change in molten salt mass in the cold tank as it enters the solar collector. If the heated salt fails to reach the desired temperature, it recirculates to the cold tank for mixing. Meanwhile, molten salt releases heat in the evaporator before returning to the cold tank. The temperature and mass changes in the cold tank are represented by (12) and (13), respectively. Equation (14) defines mass conservation in the cold tank, while (15) sets upper and lower bounds for the molten salt mass.

D. Steam Turbine Generator

The thermal exchange system includes a preheater, steam generator, superheater, and reheater. Water is preheated to near-saturation temperature, then fed into the steam generator to form saturated steam via heat exchange with high-temperature molten salt. The steam is further heated in the superheater to drive the turbine and generate electricity efficiently.

$$Q_{\text{PB,in},t} = \frac{P_t}{\eta_t} \tag{16}$$

$$\left(T_{\text{hot,out},t} - T_{\text{cold,in},t}\right) = \frac{Q_{\text{PB.in},t}}{C m_{\text{hot,out},t}} \tag{17}$$

In the equation, $Q_{\text{PB,in},t}$ represents the thermal released per unit time by the molten salt after entering the steam generator, J. P_t denotes the turbine power output at time t, J. η_t represents the thermoelectric conversion efficiency, which is positively correlated with the molten salt outlet temperature of the thermal storage tank $T_{\text{hot},\,t}$, the molten salt outlet flow rate $m_{\text{hot,out},\,t}$, and the power generation P_t. Equation (16) describes the conversion of thermal energy into electrical energy, considering a specific efficiency. After heat dissipation in the steam generator, the molten salt's temperature drops and is directed to the cold tank. This process, under a specified flow rate at the hot tank outlet, is represented by (17).

Additionally, the steam turbine operation must satisfy the following constraints:

$$u_{\text{on},t} + u_{\text{off},t} \le 1 \tag{18}$$

$$v_{t+1} - v_t = u_{\text{on},t+1} - u_{\text{off},t+1} \tag{19}$$

$$\sum_{t=0}^{\min\left(t_{\text{left}},t_{\text{on}}\right)} v_{h+t} \ge u_{\text{on},h} \min\left(t_{\text{left}},t_{\text{on}}\right) \tag{20}$$

$$\sum_{t=0}^{\min\left(t_{\text{left}},t_{\text{off}}\right)} \left(1 - v_{h+t}\right) \ge u_{\text{off},h} \min\left(t_{\text{left}},t_{\text{off}}\right) \tag{21}$$

$$P_{t+1} - P_t \ge U_{\text{up}} P_{\max}\Delta t - M u_{\text{off},t+1} \tag{22}$$

$$P_{t+1} - P_t \le U_{\text{down}} P_{\max}\Delta t + M u_{\text{on},t+1} \tag{23}$$

In the equations, the binary variable u captures operational status transitions: u_{on}=1 indicates startup, and u_{off} =1 indicates shutdown. The binary variable v indicates device status: v_t=1 is active, and v_t =0 is inactive. t_{left} is remaining scheduling time in s; t_{on} is minimum operation duration in s; t_{off} is minimum shutdown duration in s. U_{up} is the turbine's ramp-up rate in MW/h; U_{down} is the ramp-down rate in %Pe/h; $P_{\max}$ is the turbine's maximum capacity in MW. Equations (18) and (19) constrain the startup and shutdown states of the steam turbine, ensuring that only a single state transition is permitted at any given time. Equations (20) and (21) impose minimum operational and shutdown duration requirements for the steam turbine. Equations (22) and (23) limit the output variation between consecutive time steps, adhering to the turbine's ramping rate constraints.

Authorized licensed use limited to: University of Pittsburgh. Downloaded on July 07,2026 at 17:40:39 UTC from IEEE Xplore. Restrictions apply.

E. The Impact of Molten Salt Temperature on the Thermal Storage Process

The simulation process of the CSP system in this paper is shown in the flowchart in Fig.2.

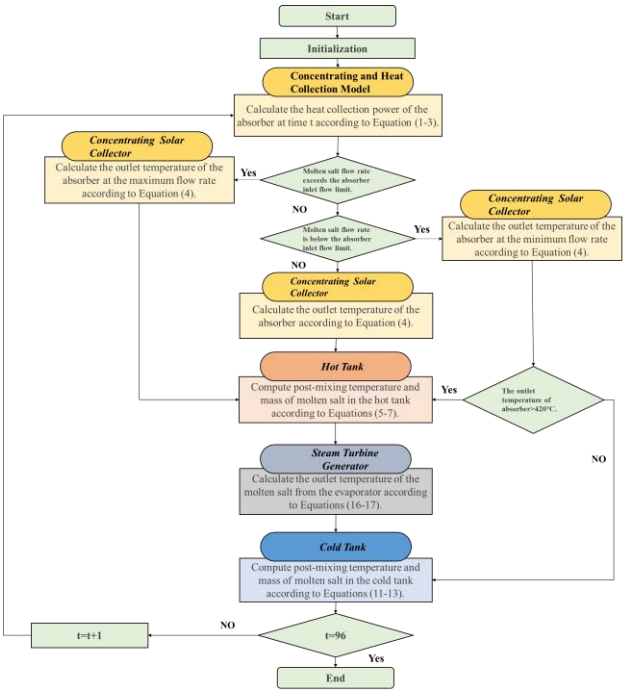

Fig. 2. Simulation calculation flowchart of CSP station

This irradiance-adaptive thermal dynamics model integrates real-time molten salt temperature evolution with flow control optimization. Daily DNI data is used to calculate the solar collector's thermal output. When solar irradiance is available, the system activates with the collector outlet set to 565°C. The molten salt flow rate from the cold tank is adjusted to achieve this temperature. If the flow exceeds the minimum threshold, the molten salt is stored in the hot tank; otherwise, it is either blended in the hot tank (if >420°C) or returned to the cold tank. During power generation, hot molten salt is pumped to the evaporator for heat exchange, then returned to the cold tank for reheating.

III. Optimization Scheduling of CSP Plants

The optimization scheduling of the CSP plant is formulated to maximize daily electricity revenue. The objective function is mathematically represented as (24). The optimization model must satisfy constraints (8)-(10) and (14)-(23).

$$\max \sum_{t=1}^{T} \left(P_t - \beta \cdot \varphi_{\text{fluc}} \right) \tag{24}$$

$$\varphi_{\text{fluc}} = \sum_{t=1}^{T} \left(P_t - P_{t\text{-}1} \right)^2 \tag{25}$$

In the equation, φ_{fluc} represents the sum of squared power differences between adjacent time points, quantifying power output fluctuation intensity.

This paper proposes a dual-layer optimization-simulation framework that decouples CSP operations into two coordinated subproblems: (1) a thermal dynamics simulation layer modeling real-time molten salt temperature evolution via irradiance-adaptive flow control, and (2) a power generation optimization layer scheduling electricity output based on the molten salt thermal state. The overall operation optimization of the CSP plant is divided into two subproblems: (1) a linear optimization model for fixed molten salt temperatures and thermal storage flow rates in the hot and cold tanks; (2) a simulation model considering variations in molten salt temperature and flow. This forms a two-layer iterative optimization framework for the CSP system. As shown in Fig. 3, based on the given molten salt flow rate curve at the hot tank outlet and the electrical load curve, the temperature and flow rate variation curves of the molten salt, as well as the thermal-electric conversion efficiency curve, are adjusted according to the plant's simulation-based operation workflow. The corrected results are then used as new boundary conditions to re-optimize the hot tank outlet flow. This iterative process continues until convergence, ultimately yielding the molten salt flow rate variation curve and the power generation curve.

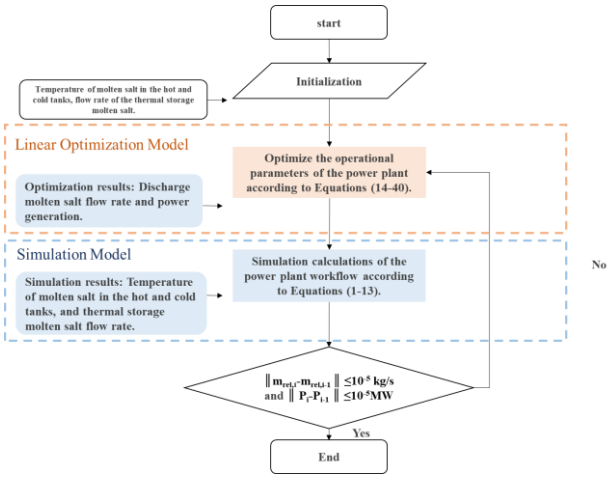

Fig. 3. Dual-Layer iterative optimization framework for CSP Plants

IV. Results and Analysis

A. Optimization Results

This study selects Guazhou County, Gansu Province (95.7890°E, 40.5344°N) as a typical location, with CSP system parameters listed in Table 1.

TABLE I. Table Type Styles

Parameter	Value
Maximum/Minimum Power Output（MW）	110/30
Ramp-up Rate（%Pe/h）	0.9
Minimum startup/shutdown duration（h）	2/2
Storage capacity（kg）	1.26×10^7
Maximum/Minimum salt storage capacity of the tank（kg）	1.13×10^7/1.26×10^7
Maximum/Minimum Discharge Flow Rate of Molten Salt（kg/s）	677.3/225.7

Authorized licensed use limited to: University of Pittsburgh. Downloaded on July 07,2026 at 17:40:39 UTC from IEEE Xplore. Restrictions apply.

The optimized dispatch results for the thermal release salt flow rate and power generation of the CSP system are shown in Fig.4, with a total power generation of 985.43 MWh.

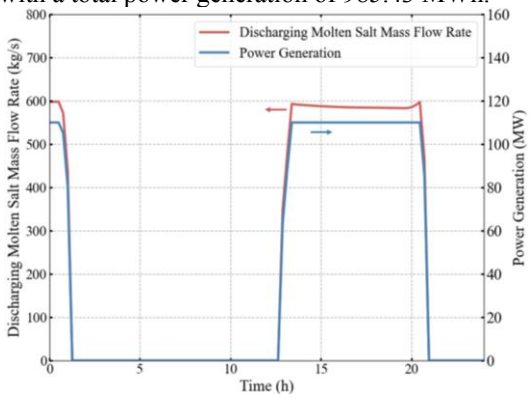

Fig. 4. Optimized thermal release salt flow rate and power generation results

The optimized results were validated using the simulation model. The collector outlet flow curve, along with the molten salt temperature and mass curves in the hot and cold tanks, are shown in Figs. 5-7.

In Fig. 6, the average molten salt temperature in the hot tank is 555.71°C. During power generation (Fig. 4), the temperature remains above this average, enhancing thermal-to-electric efficiency and system performance.

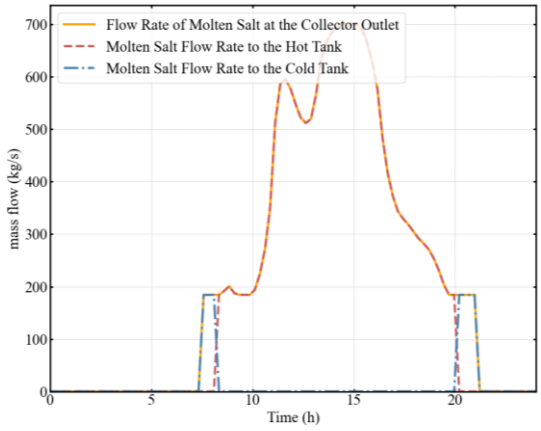

Fig. 5. The simulation results for the molten salt flow direction and flow rate at the collector outlet

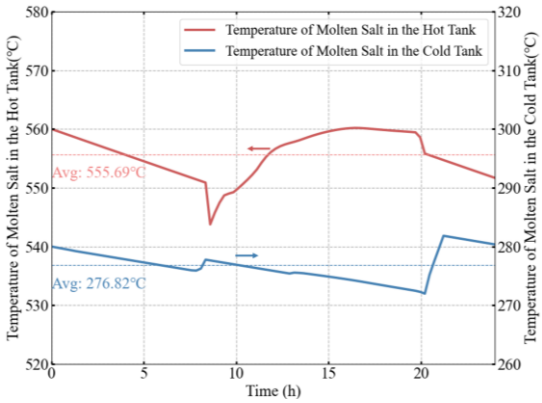

Fig. 6. The simulation results for the molten salt temperature within the hot and cold storage tanks

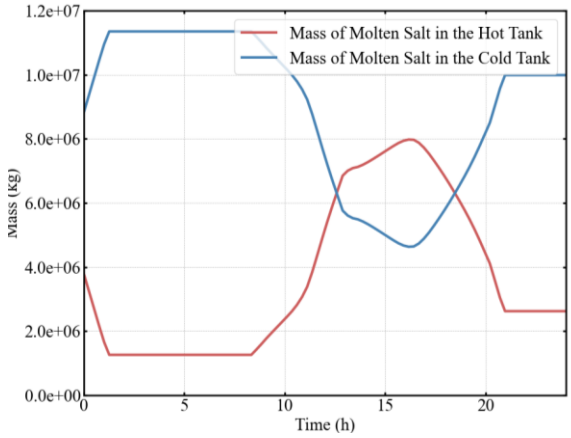

Fig. 7. The simulation results for the molten salt mass within the hot and cold storage tanks

B. *Comparison with Simplified Models*

Existing simplified CSP methods ignore molten salt temperature and flow dynamics due to storage constraints and thermoelectric efficiency variations, focusing only on energy balance. Fig. 8 compares the simplified model with this study's bi-level optimization. The simplified model achieves 935.39 MWh daily generation and a heat consumption rate of 8377.07 kJ/kWh.

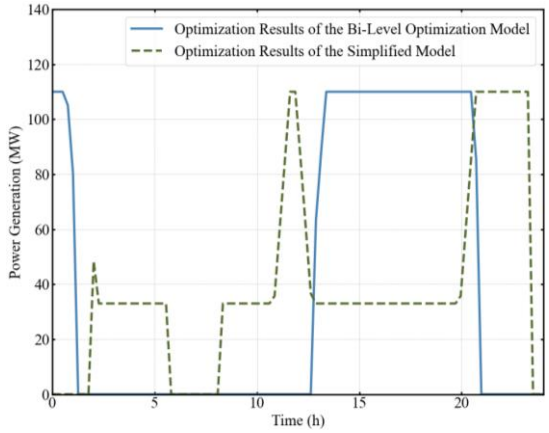

Fig. 8. Power generation optimization results for the simplified model.

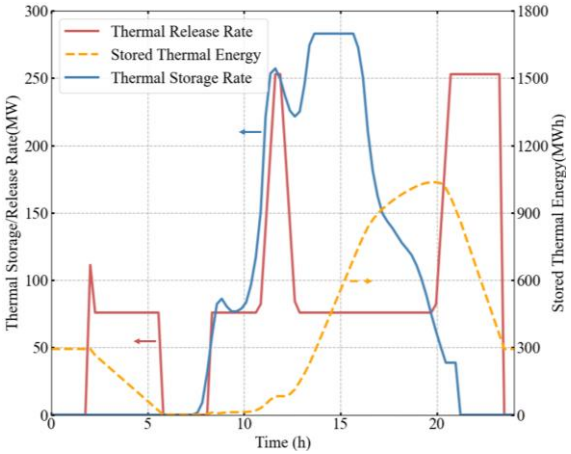

Fig. 9. Stored thermal energy and thermal storage/release rate results of the simplified model

Authorized licensed use limited to: University of Pittsburgh. Downloaded on July 07,2026 at 17:40:39 UTC from IEEE Xplore. Restrictions apply.

The dual-layer iterative algorithm, considering process constraints and efficiency variations, addresses the non-linearity of solar thermal systems, enabling real-time optimization. Daily generation is 985.43 MWh, with a heat consumption rate of 8188.32 kJ/kWh, a 2.2% reduction compared to the simplified model.

V. CONCLUSION

This study explores the optimization of molten salt tower CSP systems. Key contributions include: a modeling method considering molten salt temperature, flow, and mass variations; a simulation model under power output and release rate constraints; a dual-layer iterative optimization framework; and optimized molten salt release scheduling to maximize revenue. The approach ensures efficient scheduling by simulating flow and temperature accurately, enabling power generation when the hot tank temperature is above average. Results show daily generation of 985.43 MWh and a heat consumption rate of 8188.32 kJ/kWh, a 2.2% reduction compared to the simplified model.

REFERENCES

[1] Ma H, Sun Q, Chen Q, et al. Exergy-based flexibility cost indicator and spatio-temporal coordination principle of distributed multi-energy systems[J]. Energy, 2023, 267: 126572.

[2] Ma H, Sun Q, Chen L, et al. Cogeneration transition for energy system decarbonization: from basic to flexible and complementary multi-energy sources[J]. Renewable and Sustainable Energy Reviews, 2023, 187: 113709.

[3] Liu T, Yang J, Yang Z, et al. Techno-economic feasibility of solar power plants considering PV/CSP with electrical/thermal energy storage system[J]. Energy Conversion and Management, 2022, 255: 115308.

[4] Hamilton W T, Newman A M, Wagner M J, et al. Off-design performance of molten salt-driven Rankine cycles and its impact on the optimal dispatch of concentrating solar power systems[J]. Energy Conversion and Management, 2020, 220: 113025.

[5] Elbeh M B, Sleiti A K. Analysis and optimization of concentrated solar power plant for application in arid climate[J]. Energy Science & Engineering, 2021, 9(6): 784-797.

[6] Keyif E, Hornung M, Zhu W. Optimal configurations and operations of concentrating solar power plants under new market trends[J]. Applied Energy, 2020, 270: 115080.

[7] Khamlich I, Zeng K, Flamant G, et al. Technical and economic assessment of thermal energy storage in concentrated solar power plants within a spot electricity market[J]. Renewable and Sustainable Energy Reviews, 2021, 139: 110583.

[8] Li X, Wu X, Gui D, et al. Power system planning based on CSP-CHP system to integrate variable renewable energy[J]. Energy, 2021, 232: 121064.

[9] Li X, Gui D, Zhao Z, et al. Operation optimization of electrical-heating integrated energy system based on concentrating solar power plant hybridized with combined thermal and power plant[J]. Journal of Cleaner Production, 2021, 289: 125712.

[10] Fang Y, Zhao S. Risk-constrained optimal scheduling with combining thermal and power for concentrating solar power plants[J]. Solar Energy, 2020, 208: 937-948.

[11] Lu X, Zhou J, Omer S. Two-layer operation optimization of concentrated solar power with thermal energy storage system and soft open point[J]. International Journal of Electrical Power & Energy Systems, 2023, 146: 108788.

[12] Yang J, Yang Z, Duan Y. Load matching and techno-economic analysis of CSP plant with S–CO2 Brayton cycle in CSP-PV-wind hybrid system[J]. Energy, 2021, 223: 120016.

[13] Xiong H, Yan M, Guo C, et al. DP based multi-stage ARO for coordinated scheduling of CSP and wind energy with tractable storage scheme: Tight formulation and solution technique[J]. Applied Energy, 2023, 333: 120578.

[14] Guo Y, Ma Z, Zhang X, et al. Optimal dispatch of wind power-photovoltaic-concentrating solar power combined power generation system based on improved PSO[C]//Journal of Physics: Conference Series. IOP Publishing, 2021, 1983(1): 012060.

[15] Zhu Z, Ma X, Gu B, et al. Joint optimal scheduling model of clean energy considering CSP regulation[C]//2020 5th Asia Conference on Power and Electrical Engineering (ACPEE). IEEE, 2020: 323-328

Authorized licensed use limited to: University of Pittsburgh. Downloaded on July 07,2026 at 17:40:39 UTC from IEEE Xplore. Restrictions apply.